

A cost-effective computational technique for aeroacoustic noise prediction using the SNGR method

B. de Brye, A. Poulos, C. Legendre, G. Lielens

Free Field Technologies (part of Hexagon's Manufacturing Intelligence division),
Axis Park Louvain-la-Neuve, Rue Emile Francqui 9, B-1435 Mont-Saint-Guibert, Belgium

e-mail: benjamin.debrye@hexagon.com

Abstract

This paper presents the **SNGR** (Stochastic Noise Generation and Radiation) method. Based on RANS simulation input, this method strongly reduces the computation cost associated with the CFD simulation in comparison to direct LES-based acoustic noise source computations.

After the theoretical description of the method, this work will analyze the numerical convergence of the different parameters involved in the source generation, namely: (i) number of random samples; (ii) number of turbulent modes; and (iii) CFD cell size. The numerical efficiency will also be evaluated. To do so, the solution for a low Mach number ($M<0.1$) panel HVAC duct will be considered and compared with experimental data and acoustic predictions based on unsteady CFD simulations available in the literature.

1 Introduction

Direct computation of aeroacoustic noise sources generated by turbulent processes requires computationally costly unsteady CFD simulations, hardly affordable for industrial purposes. This high computational cost is mainly because of the disparity between the fluid dynamics and acoustic length scales. In one hand, direct noise computations must resolve both small and large eddies generating acoustic waves in the near field, requiring some mesh constraints. On the other hand, such waves must be propagated up to the far-field where a listener is placed requiring large (sometimes very extensive) computational domains. Therefore, a decoupling of the acoustic solution from the CFD simulation (commonly known as hybrid method) must be employed [1].

Even if hybrid methods may reduce the computational cost, the process remains computational expensive since it requires an accurate **Large Eddy Simulation** (LES) [2]. For example, the single calculation of a car side mirror flow could require weeks of computation on a mid-size cluster in order to reach appropriate flow statistics and resolution to compute noise sources up to the target frequency.

In contrast to LES, the steady-state Reynolds Averaged Navier-Stokes method (RANS) allows for a more cost-effective process. The main idea behind the RANS method is to parametrize the effect of sub-grid eddies on the mean flow, so that the mesh can be coarser while still maintaining good accuracy for the mean flow.

The SNGR (Stochastic Noise Generation and Radiation) method originally presented by R. Kraichnan [3] and extended by C. Bailly and D. Juvé [4] allows for the generation of noise sources using a steady-state RANS. This stochastic method synthetizes a turbulent velocity field from a finite sum of statically independent Fourier modes with modal amplitudes estimated as a function of the RANS fields, i.e. turbulent kinetic energy and turbulent dissipation rate. Afterwards, acoustic sources are computed using Lighthill's analogy. The originality of the implementation relies on: (i) the frequency/wavenumber domain approach of the velocity fluctuations; (ii) the efficient sources computation; and (iii) integration of the sources in a finite element acoustic mesh.

The present paper describes the SNGR method implemented inside Actran [5] to synthetically generate aeroacoustic sources from steady-state RANS information. Later, such sources are imposed as the right-hand side of the acoustic solver based on the finite element method. Details of the SNGR method are presented in section 2 followed by numerical demonstrations on two applications (section 3). As a first application case, an idealized pseudo-3D case (section 3.1) is used to analyze the numerical convergence of the method regarding: (i) the number of random samples; (ii) the number of turbulent modes; and (iii) the CFD mesh size. Secondly, results from an HVAC (Heating, Ventilation, and Air Conditioning) duct model (section 3.2) are compared to experimental data and classic aeroacoustic simulations (hybrid approach) with sources based on unsteady CFD solutions (LES). Finally, the computational performance of the algorithm is analyzed in section 4 followed by concluding remarks and possible future investigations (section 5).

2 Method overview

The SNGR method consists in generating a random (turbulent) velocity field as a finite sum of discrete Fourier modes based on average data of the flow field. In a second step, this turbulent velocity field is used to define source terms for acoustic propagation and radiation (either in time domain or frequency domain).

2.1 Velocity fluctuations

Let's start with the steady-state RANS simulation output providing turbulent kinetic energy \bar{k} and turbulent dissipation ϵ fields. In homogeneous turbulent flows, \bar{k} is the time average ($\langle \cdot \rangle$) of the product of the velocity fluctuations u'_j as described next:

$$\bar{k} = \frac{1}{2} \langle u'_j u'_j \rangle \quad (1)$$

and can also be analyzed in terms of its wavenumber content κ with the energy spectrum function $E(\kappa)$:

$$\bar{k} = \int_0^{\infty} E(\kappa) d\kappa. \quad (2)$$

The energy spectrum function is also used to define the turbulent dissipation rate ϵ as follows:

$$\epsilon = 2\nu \int_0^{\infty} \kappa^2 E(\kappa) d\kappa, \quad (3)$$

where ν denotes the fluid viscosity.

Once the main flow variables are defined, the turbulent velocity field (fluctuations) can be decomposed in terms of Fourier modes [4]. For this, considering a homogeneous isotropic turbulent velocity field, a time dependent formulation of the velocity fluctuation takes the form:

$$u'_j(\mathbf{x}, t) = \sum_{m=1}^N \tilde{u}(\kappa^m) \cos(\kappa_l^m (\mathbf{x} - \bar{U}_l t) + \psi^m + \omega^m t) \sigma_j^m, \quad (4)$$

where,

- κ_l^m is the wavenumber vector randomly defined on a sphere of radius κ^m associated with mode m ;
- \bar{U}_l is the local mean velocity of the flow obtained from the RANS solution;
- ψ^m is the phase of the mode m with a uniform probability distribution;
- ω^m is the angular velocity of the mode m ;
- σ_j^m is the orientation vector of the mode m . As the turbulent velocity field is supposed to be incompressible, the orientation vector σ_j^m can be defined using the continuity equation as follows:

$\partial u'_j / \partial x_j = 0 \rightarrow \sigma_j^m \cdot \kappa_l^m = 0$ for $m = 1, \dots, N$. The remaining components are set with the use of a random angles.

The angular velocity ω^m can be expressed in terms of the wavenumber κ^m using the Kolmogorov formula:

$$\omega^m = \sqrt{\frac{2\bar{k}}{3}} \kappa^m, \quad (5)$$

(by default in our implementation), or alternatively, using the Heisenberg formula:

$$\omega^m = \sqrt{\frac{3}{2}} \epsilon^{\frac{1}{3}} (\kappa^m)^{\frac{2}{3}}. \quad (6)$$

In the current implementation, the convection effects in equation (4) are neglected ($\bar{U}_l / c_0 \sim 0$ where c_0 is local speed of sound) and the velocity fluctuations are transformed to the wavenumber space using Euler's identity, i.e. $e^{ix} = \cos(x) + i \sin(x)$. Therefore, the velocity fluctuations take the following simplified form:

$$u'_j(\mathbf{x}, \kappa) = \sum_{m=1}^N \tilde{u}(\kappa^m) \exp[i(\kappa_l^m \mathbf{x} + \psi_l^m)] \sigma_j^m. \quad (7)$$

Besides, the wavenumber space is discretized using a uniform unidimensional grid ranging from 0 to $2\kappa_{\text{kol}}$ with a $\Delta\kappa$ spacing, where κ_{kol} is the Kolmogorov wavenumber, i.e. $\kappa_{\text{kol}} = (\epsilon/\nu^3)^{1/4}$. To satisfy the homogeneous isotropic turbulence properties of the synthetic flow in equation (1), each mode amplitude $\tilde{u}(\kappa_m)$ should be of the form:

$$\tilde{u}(\kappa_m) = \sqrt{\int_{\kappa_m - \frac{\Delta\kappa}{2}}^{\kappa_m + \frac{\Delta\kappa}{2}} E(\kappa) d\kappa}. \quad (8)$$

Consequently, the turbulence spectrum $E(\kappa)$ can take various forms. For instance, some authors agree on the semi-empirical von Karman – Pao spectrum [4] to express $E(\kappa)$ as follows:

$$E(\kappa) = A \frac{2\bar{k}}{3k_e} \frac{(\kappa/\kappa_e)^4}{(1 + (\kappa/\kappa_e)^2)^{\frac{17}{6}}} e^{-2(\kappa/\kappa_{\text{kol}})^2}, \quad (9)$$

where the constant A and κ_e are computed using relations (2) and (3). To illustrate the behavior of equation (9), Figure 1 plots this relation for a given set of values.

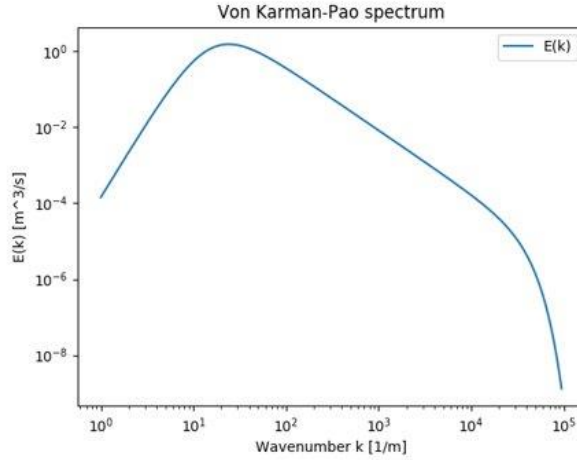


Figure 1: Von Karman Pao spectrum for $\bar{k} = 136 \text{ m}^2/\text{s}^2$, $\epsilon = 18820 \text{ m}^2/\text{s}^3$, $A = 1.47$, $k_e = 15.5 \text{ m}^{-1}$ and $k_{kol} = 47000 \text{ m}^{-1}$ in a loglog representation.

2.2 Acoustic source generation

In this work, the computation of the acoustic noise sources from the flow fluctuations is based on Lighthill's analogy [6]. This analogy is valid for low Mach number flows as no convection is considered on the acoustic operator. Lighthill's analogy is expressed as follows:

$$\frac{\partial^2 \rho}{\partial t^2} - c_0^2 \frac{\partial^2 \rho}{\partial x_j \partial x_j} = \frac{\partial^2 T_{ij}}{\partial x_i \partial x_j}, \quad (10)$$

where T_{ij} is known as the Lighthill tensor, ρ is the acoustic fluid density and c_0 is the speed of sound. For a Stokesian perfect gas like air, in an isentropic, high Reynolds number and low Mach number flow, the Lighthill tensor T_{ij} is often approximated [7] as $T_{ij} \sim \rho_0 u'_i u'_j$ where ρ_0 is the mean fluid density. In frequency domain (at angular frequency ω) and with all the previous approximations, Lighthill's analogy results in:

$$-\omega^2 \rho - c_0^2 \frac{\partial^2 \rho}{\partial x_j \partial x_j} = \rho_0 \frac{\partial^2 u'_i u'_j}{\partial x_i \partial x_j}. \quad (11)$$

Furthermore, Lighthill's analogy available in Actran is based on a finite element formalism. For this, first a change of variable is performed to express equation (11) in terms of the acoustic potential ψ , with $\rho = -i\omega\psi/c_0^2$:

$$\frac{\omega^2}{c_0^2} \psi + \frac{\partial^2 \psi}{\partial x_j \partial x_j} = \frac{\rho_0}{i\omega} \frac{\partial^2 u'_i u'_j}{\partial x_i \partial x_j}. \quad (12)$$

Then, multiplying the previous expression by a test function $\delta\psi$ and integrating by parts in the whole control volume Ω the following expression is obtained:

$$\begin{aligned} \int_{\Omega} \frac{\omega^2}{c_0^2} \psi \delta\psi d\Omega - \int_{\Omega} \frac{\partial\psi}{\partial x_j} \frac{\partial\delta\psi}{\partial x_j} d\Omega \\ = \int_{\Omega} \frac{\partial\delta\psi}{\partial x_j} \frac{\rho_0}{i\omega} \frac{\partial u'_i u'_j}{\partial x_i} d\Omega - \int_{\Gamma} \frac{\delta\psi}{i\omega} \frac{\partial}{\partial x_i} (c_0^2 \rho \delta_{ij} + \rho_0 u'_i u'_j) d\Gamma. \end{aligned} \quad (13)$$

The surface terms (integrals with sub-index Γ) in the variational formulation are used to impose or define, either: (i) acoustic boundary conditions, i.e. acoustic impedance/admittance or acoustically rigid walls (natural condition); or (ii) aeroacoustic surface sources, consequence of spatial domain truncations. By

assuming a sufficiently large domain Ω including all the sources, the surface term in equation (13) vanishes leading to a single volume source term of the form (in time or frequency domain respectively):

$$S_i(\mathbf{x}, t) \sim \rho_0 \frac{\partial u'_i u'_j}{\partial x_j} \quad \text{or} \quad S_i(\mathbf{x}, \omega) \sim \rho_0 \frac{\partial u'_i \odot u'_j}{\partial x_j}, \quad (14)$$

where \odot is the convolution product. It is worth noticing that one spatial derivative has been removed from the original Lighthill source (i.e. $\partial^2 T_{ij} / \partial x_i \partial x_j$) using the variational formulation, this is very convenient from the numerical point-of-view as second derivatives are difficult to compute from the numerical data. Secondly, the source term is a vector (instead of a scalar in the original Lighthill formulation) related to the first spatial derivative of the Reynolds's tensor, i.e. $\rho_0 u'_i u'_j$, hence a momentum source. A further simplification may be applied by using the continuity equation and given the fact that the flow is assumed to be incompressible, this results in (in time or frequency domain respectively):

$$S_i(\mathbf{x}, t) \sim \rho_0 u'_j \frac{\partial u'_i}{\partial x_j} \quad \text{or} \quad S_i(\mathbf{x}, \omega) \sim \rho_0 u'_j \odot \frac{\partial u'_i}{\partial x_j}, \quad (15)$$

or in the wavenumber space, the momentum source related to Lighthill's analogy can be expressed as:

$$S_i(\mathbf{x}, \kappa) = \rho_0 u'_j(\kappa) \odot \frac{\partial u'_i(\kappa)}{\partial x_j}. \quad (16)$$

In practice, the velocity fluctuations and momentum source are computed at the CFD cells' centers. The gradient of equation (7) is taken as follows:

$$\frac{\partial u'_i}{\partial x_j} = \sum_{m=1}^N \tilde{u}(\kappa^m) i \kappa_j^m \exp [i(\kappa_l^m x_l + \psi_l^m)] \sigma_j^m, \quad (17)$$

where the gradient of $\tilde{u}(\kappa^m)$ has been neglected as it is expected to have a little variation across the space.

To keep the SNGR method affordable in computational cost terms, the velocity fluctuations and momentum sources are evaluated at the CFD cells' centers. Consequently, the spatial fluctuations inside the CFD cells, particularly important at high wavenumber, are unresolved. Following an analytical integration of the source term inside the CFD cell to take into account the unresolved fluctuations, a multiplicative factor is determined to be proportional to $(\kappa^m)^{-3}$.

To ensure convergence with respect to the number of turbulent modes N , the source term is normalized by the factor $1/\sqrt{N}$. Besides, since the synthetically generated sources represent a statistically random process, multiple realizations constituted by different set of random numbers are necessary to ensure a correct solution level.

Finally, the sources in equation (16) are integrated on the acoustic mesh for each random number sample (realization) using equation (13) (r.h.s.- first term).

3 Application

3.1 Duct with bifurcation

As a first simplified application, a pseudo-3D model of a 2D duct with bifurcation is proposed (Figure 2). A flow of 50 m/s is imposed at the main inlet (upper-left, red domain in Figure 2) while zero flow is imposed at the secondary inlet (lower-left, blue domain in Figure 2) and zero pressure is imposed at the outlet (orange domain, Figure 2). Boundary layers are well discretized at all the walls with prismatic cells and sufficient mesh refinement is assured downstream at the bifurcation to properly capture the shear layer. The mean flow, the turbulent kinetic energy and energy dissipation rate are also plotted in Figure 3, Figure 4 and Figure 5 (respectively). The flow simulation is performed using Cradle SC/Tetra [8].

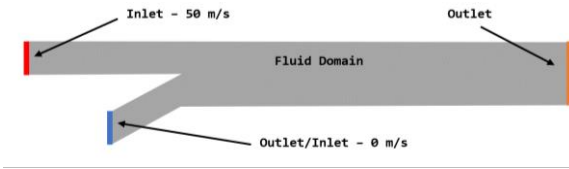


Figure 2: Sketch of the RANS inlets and outlets.

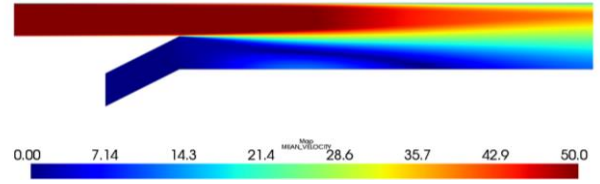


Figure 3: Mean velocity from RANS [m/s].

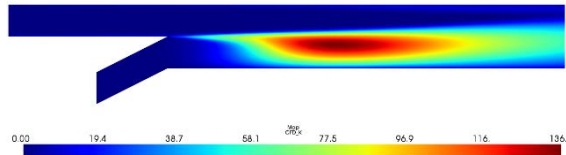


Figure 4: Turbulent kinetic energy [m²/s²].

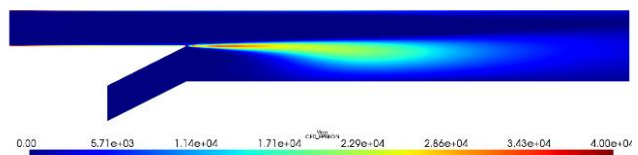


Figure 5: Turbulent dissipation rate [m²/s³].

The acoustic model covers the same area as the fluid dynamics model. Non-reflecting conditions are imposed at the inlet (blue and red domains, Figure 2) and outlet (orange domain, Figure 2) boundaries. The acoustic propagation simulation was performed in the frequency domain using the finite-element solver Actran.

Since the SNGR method relies on a random numbers generation to predict noise of a statistically steady-state process, multiple realizations or samples are needed in the simulation. Figure 6 shows the convergence of the method with the number of samples at one point located in the middle of the duct near the outlet boundary. This figure indicates that the acoustic pressure is sufficiently converged for a number of samples around 32.

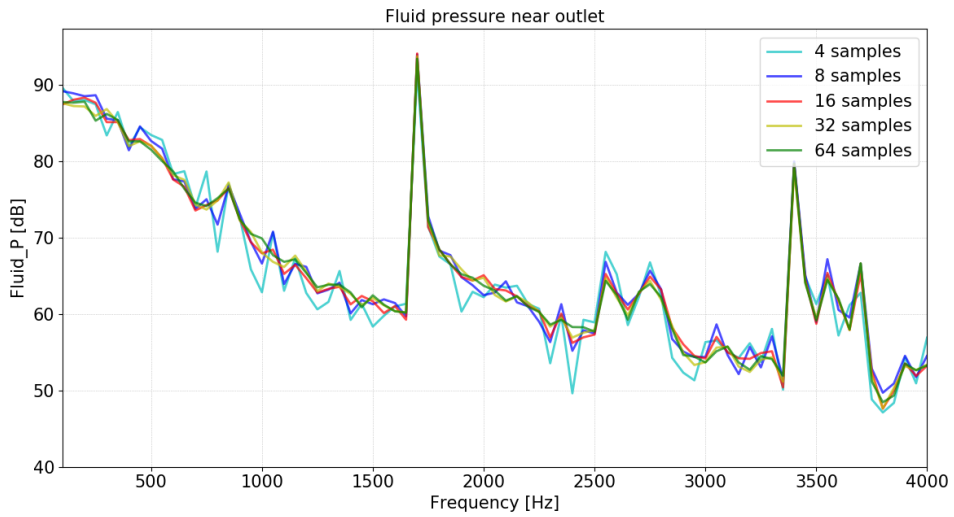


Figure 6: Convergence of the number of realizations at one microphone.

The number of turbulent modes N is a key factor for the precision of the method since it is the truncation point of the Fourier series to represent the turbulent velocity fluctuations. Indeed, numerical convergence should be achieved as the number of turbulent modes increases. In Figure 7, it is noticed that the acoustic pressure is converged even with a low number of modes except at the lowest frequencies. Indeed, the von

Karman-Pao spectrum presents a sharp peak at low wavenumber and a constant slope decrease at the middle range wavenumber (Figure 1).

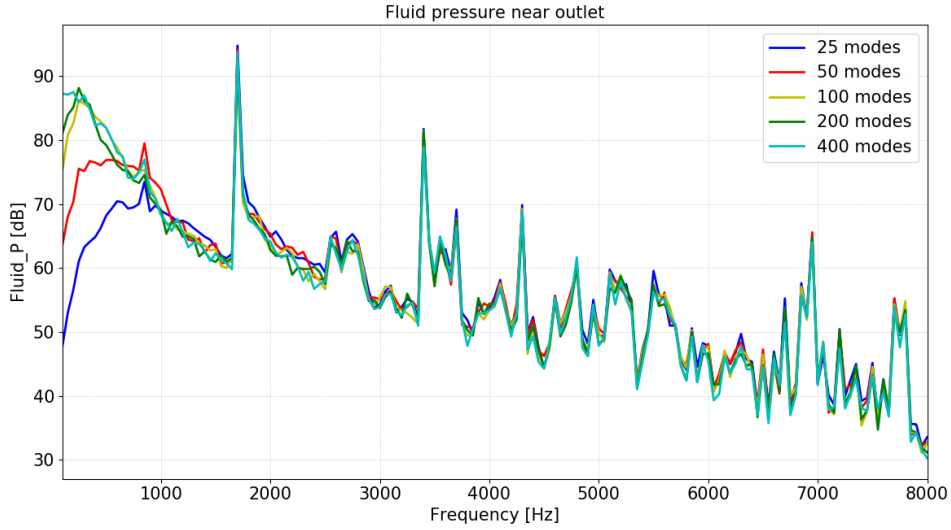


Figure 7: Convergence of the number of turbulent modes at one microphone.

The last convergence study is focused on the CFD mesh size. Certainly, the SNGR method should converge as the CFD mesh size decreases (or refinement increases). In order to highlight this process, the RANS fields were re-interpolated into different meshes with uniform mesh size ranging from 0.016 m to 0.001m. Figure 8 depicts the acoustic pressure using the various CFD meshes. Results are well superposed except at low frequencies where the missing modeling of correlation between cells starts playing a role.

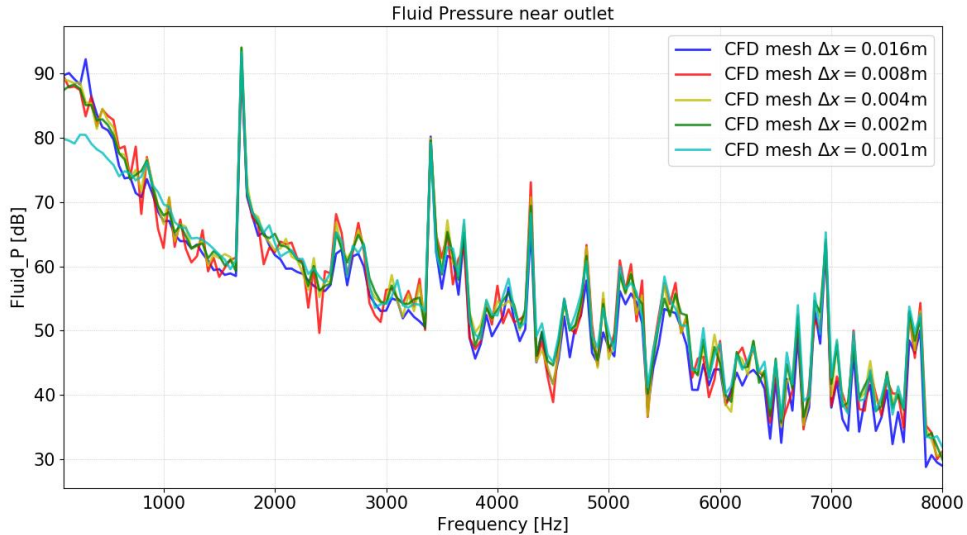


Figure 8: CFD mesh size convergence at one point.

3.2 HVAC duct model

The solution for a low Mach number ($M < 0.1$) panel HVAC duct as detailed in [9] will be considered and compared with measurement data and prediction data based on unsteady CFD results available in the literature. Ansys Fluent [10] has been used for generating the RANS solution (e.g. velocity and turbulent kinetic energy in Figure 9).

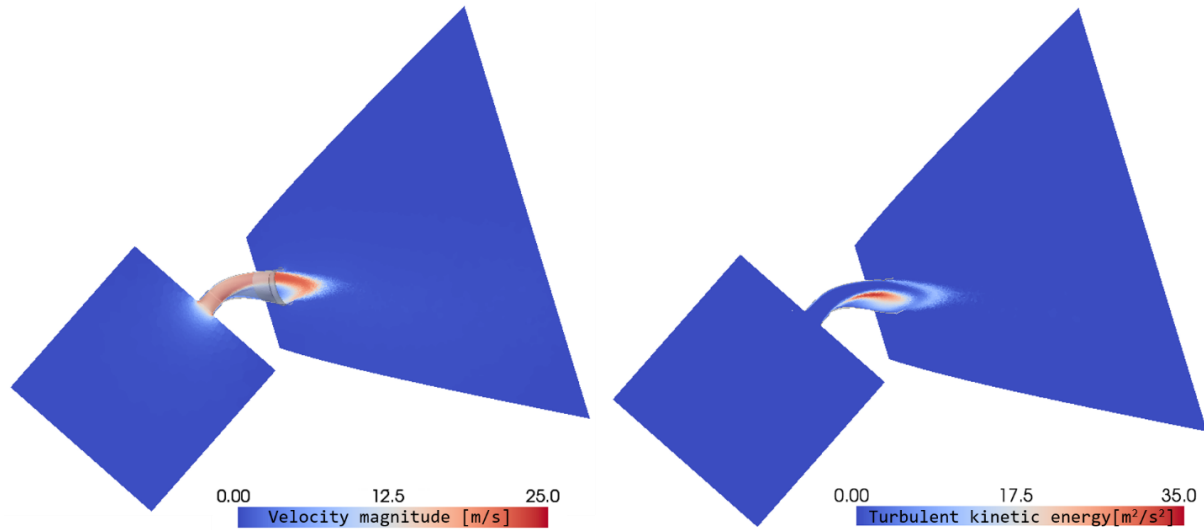


Figure 9: Velocity and turbulent kinetic energy for HVAC duct model.

The results are compared at three microphone positions as outlined in the acoustic model shown below (Figure 10):

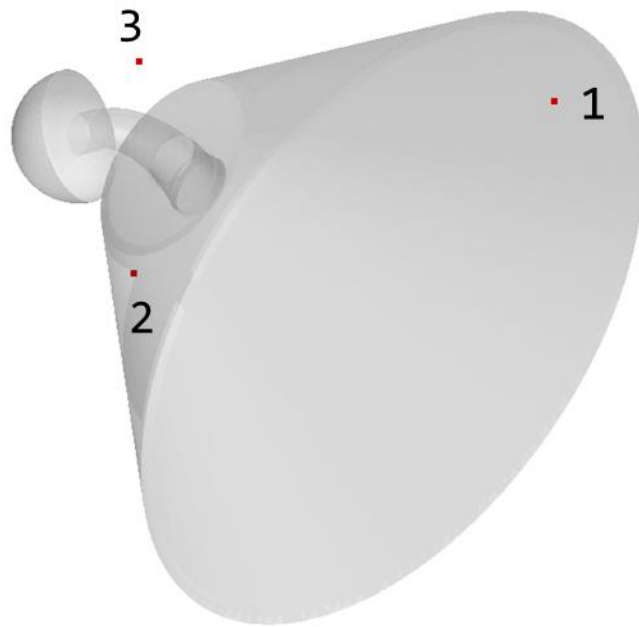


Figure 10: Acoustic model with microphone annotations.

For the SNGR simulations, a relative threshold of 0.1% has been used corresponding to neglecting the CFD cells with turbulent kinetic energy level below $0.35 \text{ m}^2/\text{s}^2$. The algorithm for automatically finding the necessary number of modes for each cell in order to properly represent the turbulent spectrum has been used with the maximum amount of modes being 256. The majority of the cells can be represented with just 16

modes and the average amount of modes is around 30. The number of random samples (realizations) used is 30.

In the plots of Figure 11, the sound pressure level can be visualized at those three microphones for frequencies up to 2000 Hz. The measurements have been averaged over a number of smaller sub-signals in order to have smoother curves. The results based on SNGR are averaged across the different realizations.

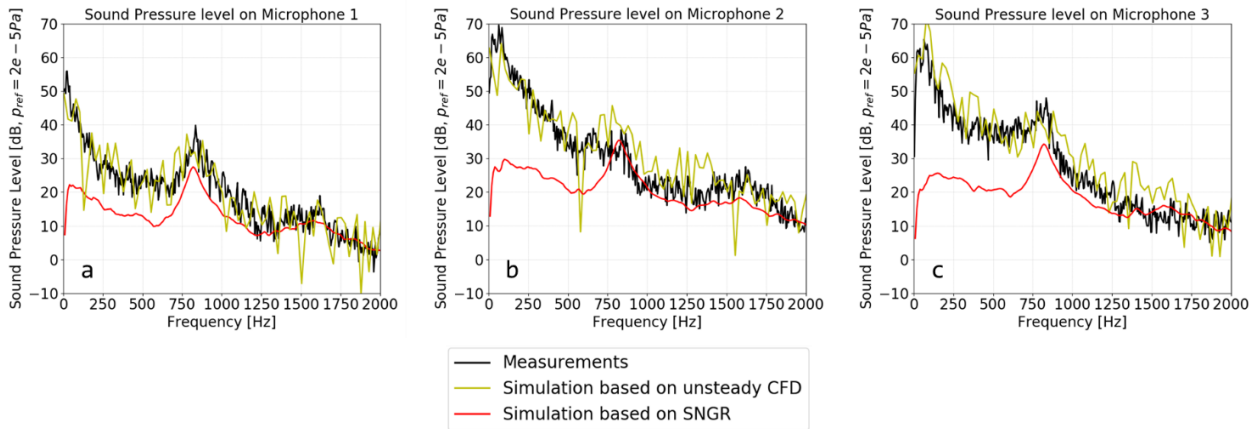


Figure 11: Sound pressure level on microphones 1 (a), 2 (b) and 3 (c).

For all three microphones, SNGR provide an accurate depiction of the higher frequency range, which is a big limitation in classic computational aeroacoustics due to the filtering of the fluctuations by the CFD mesh [11]. Also, thanks to the propagation solver, the resonance due to the duct length around 800 Hz can be properly represented. However, in the lower frequencies, even though the trend is followed, the source amplitudes lead to an underestimation of the sound pressure levels by about 10-20 dB. This discrepancy can be explained by the limitation of the von Karman-Pao spectrum law at low wavenumber. Indeed, the largest eddies are greatly dependent on the model geometry and boundary conditions, which are not parametrized in the analytical expression. Furthermore, correlations between CFD cells might play a role which is not (yet) implemented in the current SNGR method.

4 Computing performance

Computing performance is deeply dependent on the choice of implementation for the SNGR method. In the current implementation, the aeroacoustic sources are directly computed inside the wavenumber space requiring a convolution product. An initial implementation was performed by sampling the wavenumber with logarithmic spacing in order to better describe the von Karman-Pao shape (i.e. more intervals for low wavenumbers) to later compute the convolution product using an in-house implementation (directly at the target frequencies). However, it became evident that the gain in precision was largely counterbalanced by the complexity of the in-house algorithm and the computational cost of the method. The second implementation is simpler, with a linear spacing of the turbulent spectrum and the convolution product is calculated via Intel's MKL [12] package. The new implementation appeared to be one to two orders of magnitude faster.

MPI (Message Passing Interface) parallelism have been introduced in order to distribute the computing load among several processors. Since several independent realizations are needed, the parallelism has been applied on this direction. At this stage, domain parallelism is under development and it will be possible to use it combined load-case (realization) parallelism and domain parallelism. Multi-threading (using OpenMP) is also available and is very efficient since most of the computation is point-wise.

Besides, in order to reduce the peak memory allocation (mainly due to random number storage), the topological source domains can be divided into smaller ones in which iterations are done sequentially.

Likewise, filtering of the CFD cells below a certain threshold of turbulent kinetic energy level can also be applied in order to neglect cells where noise sources are small, like this memory consumption is reduced. Furthermore, by giving a threshold error for the computation of the velocity fluctuation, the number of turbulent modes can be automatically selected as a local function of the RANS fields. The latter feature allows to locally (per CFD cell) represent the turbulent velocity field with the sufficient number of Fourier modes needed.

For the HVAC model presented in section 3.2, the number of CFD cells selected is round 332 000. Each load case (realization) runs in 52 seconds using 11 processes for load-case parallelism and 4 threads per process. The full simulation time including CFD loading and post-processing reaches 9 minutes and the peak memory per process attains 5.6 GB on a 44-core Broadwell Intel Xeon chipset at 2.10 GHz.

5 Conclusions

An efficient method for the computation of aeroacoustic sources using the SNGR technique has been presented. In contrast to classic hybrid approaches in which the aeroacoustic sources are computed from computational expensive CFD simulations (LES), in the SNGR method, the sources are based on turbulent velocity fluctuations synthesized from affordable steady-state RANS simulations. The method has been described from the theoretical point-of-view and from its implementation in Actran to properly handle industrial-size applications. Because of numerous improvements, the current implementation of the method is now efficient both for the computational time and the amount of required memory.

Using a simple duct configuration, the convergence of the method was analyzed with respect to: (i) the number of random samples; (ii) the number of turbulent modes; and (ii) the CFD mesh size. Such analyses increased the confidence on the method from the numerical perspective.

A more realistic application focused on a HVAC duct has been presented. For this application, using the same numerical recipes learned from the previous case, acoustic results have been obtained and compared to experimental data and Actran simulations using sources computed with an unsteady CFD (LES). The analysis of the results (section 3.2) indicates a good correlation at middle and high frequencies with loss in accuracy at the lowest frequencies. This behavior can be explained by two reasons: (i) low frequency noise is mainly produced by large (coherent) flow structures (i.e. eddies) that are not properly resolved by the SNGR method, while high frequency noise is predominately produced by small (isotropic) eddies well synthesize by the SNGR technique; (ii) as it is depicted in Figure 1, the von Karmann-Pao spectrum is well resolved for high wavenumbers (small eddies) while is un-resolved or simply unknown a low wavenumbers.

Future developments of the method and implementations will be focused on domain parallelism, and on the improvement of prediction for low frequencies using for example extra-cell correlations (using e.g. random numbers with spatial correlation) or user-defined turbulence spectrums.

References

- [1] C. Tam, "Computational aeroacoustics issues and methods," *AIAA journal*, vol. 33, no. 10, pp. 1788-1796, 1995.
- [2] M. Cabrol, Y. Detandt and A. Talbot, "A efficient method for car exterior noise prediction based in steady CFD input.," in *ICSV 24*, London, 2016.
- [3] R. Kraichnan, "Diffusion by a random velocity field," *Physics of Fluids*, p. 13:2231, 1970.
- [4] C. Bailly and D. Juve, "A stochastic approach to compute subsonic noise using linearized Euler'sequations," 5th AIAA/CEAS Aeroacoustics Conference and Exhibit, p. 1872, 1999.
- [5] Actran, "www.fft.be," Free Field Technologies (part of Hexagon's MI), 2020. [Online].

- [6] M. J. Lighthill, "On sound generated aerodynamically," *Proceedings of the Royal Society A*, vol. Volume A, no. 211, 1952.
- [7] M. Goldstein, *Aeroacoustics*, McGraw–Hill, 1976.
- [8] Cradle Co., "ScTetra Version 13, User's guide, Basic of CFD Analysis," 2017.
- [9] J. Manera, Y. Detandt, D. d'Udekem and S. Détry, "Aero-Acoustic Predictions of Automotive Instrument Panel Ducts," *SAE Technical Papers*, vol. 1, 2009.
- [10] Ansys Fluent, "Fluent 11.0 User's Guide".
- [11] A. Pietrzyk, D. Beskow, D. Moroianu, M. Cabrol and Y. Detandt, "Passenger car side mirror exterior noise simulation and validation," in *ICSV 22*, Florence, 2015.
- [12] MKL, "Intel Math Kernel Library," Intel, 2020. [Online]. Available: <https://software.intel.com/content/www/us/en/develop/tools/math-kernel-library.html>.